Characterization of Sodium Cobalt Oxides Related to P3-Phase Superconductor

Kazunori Takada,*[,†,§] Minoru Osada,[†] Fujio Izumi,[†] Hiroya Sakurai,[‡] Eiji Takayama-Muromachi,[‡] and Takayoshi Sasaki[†,§]

Advanced Materials Laboratory and Superconducting Materials Center, National Institute for Materials Science, 1-1 Namiki, Tsukuba, Ibaraki 305-0044, Japan, and Japan Science and Technology Agency (JST), 4-1-8, Honcho, Kawaguchi, Saitama 332-0012, Japan

Received December 24, 2004. Revised Manuscript Received February 20, 2005

This paper reports characterization of sodium cobalt oxides related to a P3-phase superconductor (space group $R\bar{3}m$) newly found other than P2 phase (space group $P6_3/mmc$). α-$NaCoO_2$ used as a parent compound for the synthesis of the superconductor was oxidized to be $Na_{0.42}CoO_2$, in which the rhombohedral structure in the parent phase providing octahedral coordination environment for Na^+ ions changed to a monoclinic lattice with trigonal prismatic sites. Hydration of the as-oxidized $Na_{0.42}CoO_2$ to the superconducting bilayer-hydrate phase was accompanied by the ion exchange between Na^+ and H_3O^+ ions and reductive insertion of H_3O^+ ions as observed in the formation of P2-phase superconductor. Partial dehydration of the superconducting phase transformed its bilayer-hydrate structure into a monolayer-hydrate one, in which the superconductivity disappeared again. Influence of the decreasing interlayer distance caused by the dehydration upon the guest species is discussed in combination with the results of Raman spectroscopy.

Introduction

A sodium cobalt oxide with bilayer-hydrate (BLH) structure was the first superconductor in a cobalt oxide system.[1] The superconducting cobalt oxide is composed of CoO_2 layers built up from CoO_6 octahedra sharing their edges and insulating layers composed of guest species interposed between them. The interesting properties may arise from the triangular arrangement of Co ions[2] and strongly correlated electrons whose structure reflects Kagomé lattice hidden in the triangular lattice.[3] Therefore, most of the studies for the elucidation of the superconductivity from a physicists' standpoint have been focused on the inside of the CoO_2 layer.

However, insight only into the CoO_2 layer will never lead us to the elucidation, because there are related nonsuperconducting materials despite the identical CoO_2 layers in them. The superconducting BLH-phase was synthesized from γ-$Na_{0.7}CoO_2$[4] as a parent compound by two-step soft-chemical modification involving partial extraction of Na^+ ions in a bromine/acetonitrile solution and sebsequent hydration of the oxidized powder in water. The oxidation process decreased the Na content with a minor change in the structure; for example, the interlayer distance slightly increased from 5.5 to 5.6 Å. Neither the anhydrous (AH) parent nor the as-oxidized phase is superconducting. In the following hydration process, H_2O molecules were inserted into the compound and coordinated to the Na^+ ions to form double layers in the galleries, which propped up the CoO_2 layers to increase the interlayer distance largely to 9.8 Å, inducing superconductivity. Partial dehydration of the BLH-phase resulted in a monolayer-hydrate (MLH) phase, in which H_2O molecules and Na^+ ions are on the intermediate plane between the CoO_2 layers.[5] This decreases the interlayer distance from 9.8 to 6.9 Å with disappearance of the superconductivity.[5,6]

Comparison between these phases revealed that the CoO_2 layer with optimum carrier density is not sufficient to induce the superconductivity. Besides the very similar CoO_2 layers in structure, a nonsuperconducting phase sometimes has the same oxidation state of Co, which corresponds to the carrier density in the CoO_2 layer, as the superconducting counterpart. For instance, the carrier density in the nonsuperconducting MLH-phase should be the same as that in the superconducting BLH-phase, because the partial removal of H_2O molecules transforming the BLH-phase into the MLH-phase never changes the carrier density. Moreover, Co oxidation states of the superconducting phase in recent studies range from +3.26 to +3.46.[7−9] Even the Co oxidation state in the parent γ-$Na_{0.7}CoO_2$ (+3.30) falls in this range; however, it

* To whom correspondence should be addressed. Tel: +81-29-860-4317. Fax: +81-29-854-9061. E-mail: takada.kazunori@nims.go.jp.
† Advanced Materials Laboratory, National Institute for Materials Science.
‡ Superconducting Materials Center, National Institute for Materials Science.
§ CREST, Japan Science and Technology Agency.

(1) Takada, K.; Sakurai, H.; Takayama-Muromachi, E.; Izumi, F.; Dilanian, R. A.; Sasaki, T. *Nature* **2003**, *422*, 53.
(2) Badding, J. *Nat. Mater.* **2003**, *2*, 208.
(3) Koshibae, E.; Maekawa, S. *Phys. Rev. Lett.* **2003**, *91*, 257003.
(4) Fouassier, C.; Matejka, G.; Reau, J.-M.; Hagenmuller, P. *J. Solid State Chem.* **1973**, *6*, 532.
(5) Takada, K.; Sakurai, H.; Takayama-Muromachi, E.; Izumi, F.; Dilanian, R. A.; Sasaki, T. *J. Solid State Chem.* **2004**, *177*, 372.
(6) Foo, M. L.; Schaak, R. E.; Miller, V. L.; Klimczuk, T.; Rogado, N. S.; Wang, Y.; Lau, G. C.; Craley, C.; Zandbergen, H. W.; Ong, N. P.; Cava, R. J. *Solid State Commun.* **2003**, *127*, 33.
(7) Karppinen, M.; Asako, I.; Motohashi, T.; Yamauchi, H. *Chem. Mater.* **2004**, *16*, 1693.
(8) Takada, K.; Fukuda, K.; Osada, M.; Nakai, I.; Izumi, F.; Dilanian, R. A.; Kato, K.; Takata, M.; Sakurai, H.; Takayama-Muromachi, E.; Sasaki, T. *J. Mater. Chem.* **2004**, *14*, 1448.
(9) Milne, C. J.; Argyriou, D. N.; Chemseddine, A.; Aliouane, N.; Veira, J.; Landsgesell, S.; Alber, A. *Phys. Rev. Lett.* **2004**, *93*, 247007.

10.1021/cm047737y CCC: $30.25
Published on Web 03/24/2005

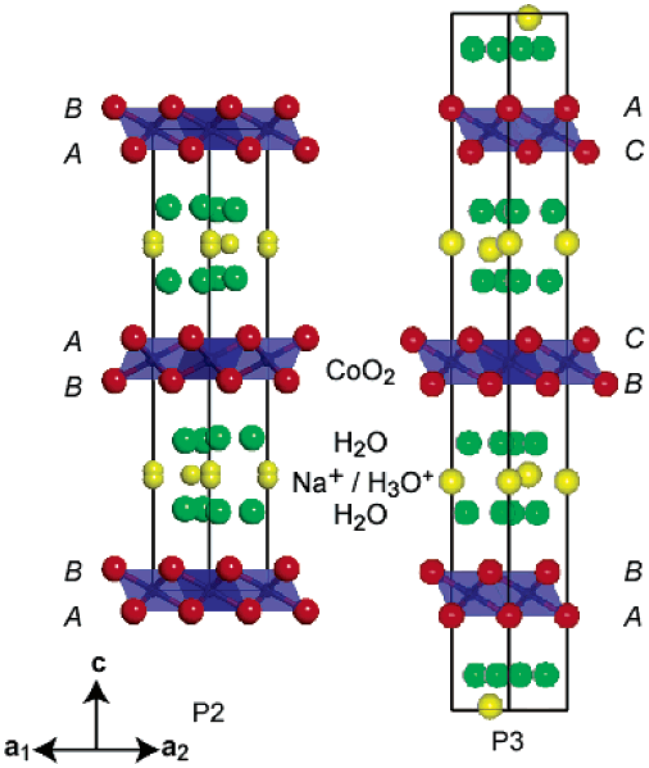

Figure 1. Crystal structures of the P2 and P3 superconductors. *A*, *B*, and *C* denote positions of oxygen atoms in hexagonal sheets.

is not superconducting indeed. Consequently, what induces the superconductivity may be found not in the CoO_2 layers but, for example, in the arrangement of the guest species. Of course, the most distinguished difference between the related materials is in the interlayer distance, which is caused by the different arrangement of the guest species. Only the BLH-phase with the largest interlayer distance shows superconductivity; therefore, the two-dimensionality enhanced by the large separation between the CoO_2 layers is believed to play an important role for inducing the superconductivity. However, there is another possibility that the arrangement of the guest species itself is a predominant factor. Na^+ ions reside near oxygen atoms in the CoO_2 layers in the AH and MLH-phases, while H_2O molecules are interposed between them in the BLH-phase. They may shield the CoO_2 layers from the random coulomb potential generated by the positively charged Na^+ ions to induce the superconductivity.[10] That is the reason characterization of such related materials to clarify the difference is still important to understanding the superconducting mechanism.

Only the BLH-phase had been a superconducting cobalt oxide for the comparative study with nonsuperconducting ones. We recently found another superconducting phase of cobalt oxide,[11] which was obtained from α-$NaCoO_2$[4] in place of γ-$Na_{0.7}CoO_2$ for the previous superconductor. The previous superconductor has P2 structure (hereinafter referred as to P2 phase displayed in Figure 1 left), in which CoO_2 layers are stacked with two-layer periodicity, and oxygen atoms in the adjacent CoO_2 layers form trigonal prismatic sites in the galleries. The new superconductor has three CoO_2 layers in the unit cell, being categorized as P3 structure (Figure 1 right; hereinafter referred as to P3 phase). The P3 phase superconductor has many similarities to the P2 one. Despite the different stacking sequence of the CoO_2 layers, its crystal structure is very similar to that of the P2 counterpart; Na^+ ions and H_3O^+ ions are on the intermediate plane between the CoO_2 layers, coordinated with H_2O molecules forming double layers in the galleries. The chemical composition including the Co oxidation state was also similar, and the P3 phase showed superconducting transition at almost the same temperature (4.6 K) and a similar superconducting volume fraction (12% and 13% at 2 K for the P3 and P2 phases, respectively). The P3 phase superconductor has several related materials as the P2 one does. Comparison between them will lead us to better understanding of the superconductivity. The objective of the present study is characterization of the related materials for the comparative study. Very recently, a hydrous sodium cobalt oxide was reported to have crystal structure and composition very similar to the P3 phase superconductor.[12] Despite the similarity, superconductivity was, surprisingly, not observed. The results of the present characterization of the nonsuperconducting materials may explain why the hydrate is not superconducting.

Experimental Section

Synthesis. Three kinds of sodium cobalt oxides, the P3-phase superconductor and its related phases, were synthesized: anhydrous (AH), or as-oxidized, Na_xCoO_2, which was obtained by chemical oxidation of α-$NaCoO_2$; BLH-Na_xCoO_2 showing superconductivity, which was obtained by the immersion of the AH-Na_xCoO_2 in water; and MLH-Na_xCoO_2, which was obtained by partial removal of H_2O molecules from BLH-Na_xCoO_2.

First of all, α-$NaCoO_2$ used as a parent oxide was synthesized according to the procedure reported in ref 4. Stoichiometric amounts of Na_2O_2 and Co_3O_4 were mixed and heated at 600 °C under an oxygen gas flow for 8 h. The obtained sample was ground and immersed in an acetonitrile solution of bromine for 5 days to extract part of Na^+ ions. Ten-fold excess of bromine with respect to the Na content was used for the oxidation. After that, it was washed with acetonitrile and dried under an argon gas flow to obtain AH-Na_xCoO_2. The AH-Na_xCoO_2 was hydrated to be BLH-Na_xCoO_2 by the immersion in distilled water for 1 day. The BLH-Na_xCoO_2 was then partially dehydrated in a nitrogen gas atmosphere for one week to obtain MLH-Na_xCoO_2.

In contrast to the materials belonging to the P3 series, materials related to the P2 superconductor, P2 BLH- and P2 MLH-phases, were synthesized as previously reported.[1,5]

Chemical Analysis. The chemical composition of the materials was determined by inductively coupled plasma atomic emission spectroscopy (ICP−AES) and redox titration. A weighed amount of the samples was dissolved in a HCl solution for ICP−AES. Redox titration was performed using sodium oxalate, $(COONa)_2$, as a reducing agent. After the sample was dissolved in a HCl solution containing an excess amount of $(COONa)_2$, residual $(COONa)_2$ was titrated by an aqueous solution of potassium permanganate ($KMnO_4$) to deduce the oxidation state of Co ions.

(10) Sakurai, H.; Takada, K.; Izumi, F.; Dilanian, R. A.; Sasaki, T.; Takayama-Muromachi, E. *Physica C* **2004**, *421*−*414*, 182.
(11) Takada, K.; Sakurai, H.; Takayama-Muromachi, E.; Izumi, F.; Dilanian, R. A.; Sasaki, T. *Adv. Mater.* **2004**, *16*, 1901.
(12) Mistry, S.; Arnold, D. C.; Nuttall, C. J.; Lappas, A.; Green, M. A. *Chem. Commun.* **2004**, 2440.

The compositions of the hydrates were calculated on the basis of a chemical formula, $Na_x(H_3O)_y(H_2O)_zCoO_2$, where the Na content, x, was determined by the ICP−AES. The oxonium content, y, was calculated using the equation, $4 - x - y = V(\mathrm{Co})$, where $V(\mathrm{Co})$ denotes an oxidation state of Co determined by the redox titration. The water content, z, was calculated by attributing it to the residual mass resulting from the x and y, instead of its direct determination. It is known that z determined directly by infrared spectroscopy for the evolved species from a heated sample well agrees with the calculated value.

X-ray Powder Diffraction Measurements and Structure Refinements. XRD data for P3 MLH-phase were collected on a Bragg−Brentano-type diffractometer (RINT Ultima$^+$, Rigaku) with Cu Kα radiation. The sample was placed in a sample chamber in which the temperature and relative humidity were maintained at 25 °C and 3%, respectively, during the measurement. In case of AH-Na_xCoO_2, the sample holder was covered with an aluminum window to prevent the exposure of the sample to humid air. The XRD data were measured in a 2θ range from 5.0 to 140.0° with a step of 0.02°.

The structure refinements were carried out by the Rietveld and maximum-entropy methods (MEM) using the computer programs RIETAN-2000[13] and PRIMA,[14] respectively. Observed structure factors, F_o(Rietveld)s, were estimated on the basis of the result of the Rietveld analysis according to Rietveld's procedure,[15] and then they were analyzed by MEM to yield electron-density distribution over a unit cell. The whole powder pattern calculated by fixing structure factors at F_c(MEM)s, which were structure factors evaluated by the Fourier transform of the electron densities, was fitted to the observed one to refine parameters irrelevant to the structure (MEM-based whole-pattern fitting: MPF).[16] After that, electron-density distribution was determined again by MEM using F_o(wpf)s estimated after the whole-pattern fitting in the same manner as the calculation of F_o(Rietveld)s. In such a manner, MEM analysis and whole-pattern fitting were alternately carried out until R factors in the latter no longer decreased appreciably (REMEDY cycles).[16]

Raman Spectroscopy. Raman spectra were recorded in a backward microconfiguration, using a 514.5-nm line from an Ar^+ laser (~0.1 mW) focused to a 2-μm-diameter spot on individual grains of the samples. The scattered light was dispersed by a subtractive triple spectrometer (T64000, Jobin-Yvon/Atago Bussan) and collected with a liquid nitrogen cooled charge-coupled device (CCD) detector.

Magnetization Measurement. The magnetizations of the samples were measured by a superconducting quantum interference device (SQUID) magnetometer (MPMS-XL, Quantum Design). They were measured under zero-field-cooling condition and a magnetic field of 10 Oe.

Results and Discussion

Na Deintercalation from α-$NaCoO_2$. The chemical analyses revealed that the chemical composition of the AH-phase obtained from α-$NaCoO_2$ was $Na_{0.42}CoO_2$, which was in coincidence with that of an anhydrous (P2 AH-) phase obtained from γ-$Na_{0.70}CoO_2$ ($Na_{0.41}CoO_2$) by the same procedure.[8] The x achieved by the chemical oxidation is governed by the oxidation power of bromine; that is, x decreases until the redox potential of the Co^{4+}/Co^{3+} couple, $E(Co^{4+}/Co^{3+})$, in AH-Na_xCoO_2 becomes equal to that of Br^-/Br_2 couple. The structure of the CoO_2 layer is very similar between the P2 and P3 AH-phases, which is considered to result in the same compositions in their as-oxidized phases. The difference in layer stacking hardly affects the redox behavior. In fact, electrochemical deintercalation of Na^+ ions from α-$NaCoO_2$[17] was reported to show a composition dependence of the $E(Co^{4+}/Co^{3+})$ similar to that for γ-$Na_{0.7}CoO_2$.[18]

Table 1. Fractional Coordinates, Occupancies, *g*, and Isotropic Atomic Displacement Parameters, *U*, for the AH-Phase[a]

atom	site	x	y	z	g	U/Å^2
Co	2*a*	0	0	0	1	0.0034(3)
O	4*i*	0.3879(5)	0	0.1703(3)	1	0.0078(5)
Na	8*j*	0.8113(18)	0.088(4)	0.4911(11)	0.106	0.010(3)

[a] Space group $C2/m$ (No. 12); $a = 4.8700(5)$ Å, $b = 2.8101(3)$ Å, $c = 5.8265(6)$ Å, and $\beta = 105.586(4)°$; $R_{wp} = 11.33\%$ ($S = 1.50$), $R_p = 7.68\%$, $R_B = 2.87\%$, and $R_F = 2.46\%$. The Na content was fixed at the value determined by the ICP-AES analysis in the refinement.

The oxidative deintercalation also brought about structural changes. The reflections from the AH-Na_xCoO_2 were not indexable on a hexagonal or rhombohedral lattice, which the other related phases in the series adopt. For example, clearly-split reflections were observed at the diffraction angles where the 107 and 018 reflections on a rhombohedral lattice are expected. This strongly suggests the distortion into monoclinic structure. Actually, a satisfactory structure refinement was achieved using a structure model with a space group of $C2/m$ based on β-$Na_{0.67}CoO_2$.[19] Table 1 lists the refined structure parameters, and Figure 2 a shows the Rietveld refinement patterns. The final R factors were low enough, which further decreased to be $R_{wp} = 11.14\%$ ($S = 1.47$), $R_p = 7.50\%$, $R_B = 1.58\%$, and $R_F = 1.22\%$ after two REMEDY cycles, to support this structure model.

The CoO_2 layers in α-$NaCoO_2$ laterally glided with respect to each other upon the deintercalation to change the Na coordination environment from octahedral to trigonal prismatic as displayed in Figure 3. The Co ions in starting α-$NaCoO_2$ are in trivalent state and low spin ($S = 0$) with $(t_{2g})^6$ configuration. The deintercalation generates Co^{4+} ions with $(t_{2g})^5$ having a spin $^1/_2$, which will distort CoO_6 octahedra by Jahn−Teller effect, lowering the symmetry from $R\bar{3}m$ to $C2/m$. The distortion was slight: lattice parameters of a monoclinic cell deduced from an ideal rhombohedral one with the cell volume and the interlayer distance corresponding to the observed monoclinic cell of the AH-phase were $a = 4.87$ Å, $b = 2.81$ Å, $c = 5.84$ Å, and $\beta = 106.1$ °, which are only slightly different from the observed value. The AH-phase can be categorized into P′3 structure.

The oxidation state of Co in the AH-phase should be +3.58 that can be deduced from the Na content of 0.42,

(13) Izumi, F.; Ikeda, T. *Mater. Sci. Forum* **2000**, *321−324*, 198.
(14) Izumi, F.; Dilanian, R. A. *Recent Research Developments in Physics, Vol. 3, Part II*; Transworld Research Network: Trivandrum, India, 2002; pp 699−726.
(15) Rietveld, H. M. *J. Appl. Crystallogr.* **1969**, *2*, 65.
(16) Izumi, F.; Kumazawa, S.; Ikeda, T.; Hu, W.-Z.; Yamamoto, A.; Oikawa, K. *Mater. Sci. Forum* **2001**, *378−381*, 59.
(17) Kikkawa, S.; Miyazaki, S.; Koizumi, M. *J. Power Sources* **1985**, *14*, 231.
(18) Braconnier, J.-J.; Delmas, C.; Fouassier, C.; Hagenmuller, P. *Mater. Res. Bull.* **1980**, *15*, 1797.
(19) Ono, Y.; Ishikawa, R.; Miyazaki, Y.; Ishii, Y.; Morii, Y.; Kajitani, T. *J. Solid State Chem.* **2002**, *166*, 177.

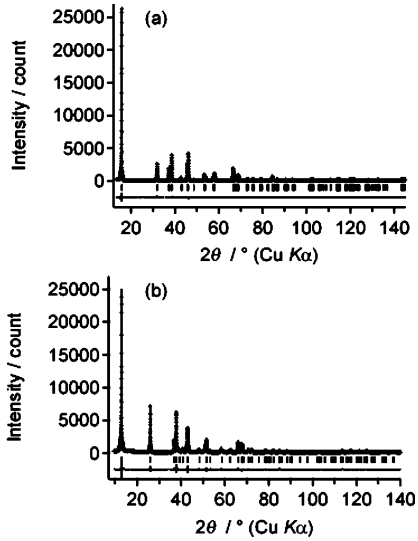

Figure 2. Rietveld refinement patterns for the AH- (a) and MLH- (b) phases in the P3 series. The observed diffraction intensities and the calculated patterns are represented by plus signs and solid lines, respectively. The curves at the bottom represent the difference. Short bars below the observed and calculated patterns indicate the positions of allowed Bragg reflections.

because only deintercalation of Na^+ ions took place during the oxidation process. However, a lower value of +3.51 was obtained by the redox titration. The reason for this discrepancy will be a high $E(Co^{4+}/Co^{3+})$ exceeding the oxidation potential of water. Not only $(COONa)_2$, which was used as a reducing agent, but also the water in the aqueous HCl solution used in the analysis should be oxidized owing to the high $E(Co^{4+}/Co^{3+})$, which resulted in a smaller consumption of $(COONa)_2$ and thus the underestimation of the Co oxidation state. In fact, the oxidation state estimated from bond-valence calculation[20] based on the Co−O bond lengths (1.8801(12) Å × 4 and 1.8913(5) Å × 2) was +3.65, suggesting that the Co ions should have an oxidation state higher than that determined by the redox titration. Similar deviation was observed for AH-phase obtained from γ-$Na_{0.7}CoO_2$, i.e., AH-phase with P2 stacking. The oxidation states of the AH-samples were reported to be +3.56[8] and +3.48,[7] which were lower than +3.60 and +3.64, respectively, expected from their Na contents ($x = 0.40$ in ref 8 and $x = 0.36$ in ref 7).

Hydration Process from AH- to BLH-Phase. It had been believed that only the insertion of H_2O molecules takes place during the transformation process from AH- into BLH-phase in P2 series. However, our recent study demonstrated that Na^+/H_3O^+ ion-exchange and reductive insertion of H_3O^+ ions proceed as well; the former decreases the Na content and the latter lowers the Co oxidation state.[8] The similar phenomena were observed in the present P3 system. The Na content was decreased from 0.42 in the AH-phase to 0.36 in the BLH-one. The Co oxidation state in the P3 BLH-phase was analyzed to be +3.48,[11] which was lower than +3.58 in the AH-phase. It should be noted that the Co oxidation state in the hydrates determined by the titration method was much more reliable than that in the AH-phases. Since the hydrates had been brought into contact with water, water in the aqueous solution used for the analysis should not promote further reduction of the Co ions.

The reduction of the Co ions was reported to be promoted by the high $E(Co^{4+}/Co^{3+})$ in the AH-phase for the P2 series.[8] When the AH-phase was immersed in water, H_2O molecules were inserted into its galleries, and simultaneously, part of the Na^+ ions were exchanged with H_3O^+ ions. The ion exchange resulted in an aqueous solution of NaOH. The increasing pH should make the oxidation potential of water lower[21] than $E(Co^{4+}/Co^{3+})$ in Na_xCoO_2, which will promote the reduction of the Co ions accompanied by additional insertion of H_3O^+ ions. Since the above process is dominated by $E(Co^{4+}/Co^{3+})$, it should proceed in the P3 counterparts in the same way. Large separation between the adjacent CoO_2 layers by a thick insulating layer in the BLH-phases should make their correlation much weaker than that in the AH-phase, resulting in the same compositional dependence of $E(Co^{4+}/Co^{3+})$ between the P2 and P3 BLH-phases and thus the similar formation process despite the different stacking.

The charge balancing species for the reduction was reported to be H_3O^+ ions for the P2 phases,[8] which will stand for the P3 ones. The presence of H_3O^+ ions was evidenced by Raman spectroscopy as will be described later.

The formation of the BLH-phase changed not only the composition but also the crystallographic symmetry. The higher symmetry (rhombohedral) was recovered in the BLH-phase. The decrease in Co^{4+} ions should be responsible for the release of the distortion.

Partial Dehydration of the P3 BLH-Phase. Figure 4 shows the XRD patterns for the P3 superconducting (BLH-) phase and the sample after the dehydration (P3 MLH-phase). The drying in N_2 gas atmosphere yielded a new layered phase with a basal spacing of 6.9 Å as observed in dehydration of the P2-phase superconductor.[5,6]

The transformation from the BLH-phase to the MLH-phase quenched the superconductivity as observed in P2 series.[5,6] Figure 5 shows the magnetic susceptibilities for the P3 MLH-sample as well as the P3 BLH-sample. The P3 MLH-phase did not show superconducting transition down to 1.8 K.

The Na content and the Co oxidation state in the P3 MLH-phase were 0.36 and +3.49, respectively, which lead to the composition of $Na_{0.36}(H_3O)_{0.15}(H_2O)_{0.44}CoO_2$. The composition and the Co oxidation state of the P3 BLH-phase were $Na_{0.35}(H_3O)_{0.17}(H_2O)_{1.22}CoO_2$ and +3.48, respectively;[11] that is, the Na and oxonium contents practically remained unchanged upon the dehydration. On the other hand, the H_2O content decreased from 1.22 to 0.44. The decrease corresponds to the weight loss of 11%, which well agreed with the observed weight loss by the dehydration (12%). These results support the fact that the reaction during the drying is only partial removal of H_2O molecules.

There was no change in crystallographic symmetry in this dehydration process. All the reflections for the MLH-phase were indexable on a rhombohedral cell with a space group of $R\bar{3}m$. Two modes of layered stacking are possible with this space group: one is P3 phase and the other is O3 phase.

(20) Brown, I. D.; Altermatt, D. *Acta Crystallogr. B* **1985**, *41*, 244.

(21) Li, W.; McKinnon, W. R.; Dahn, J. R. *J. Electrochem. Soc.* **1994**, *141*, 2310.

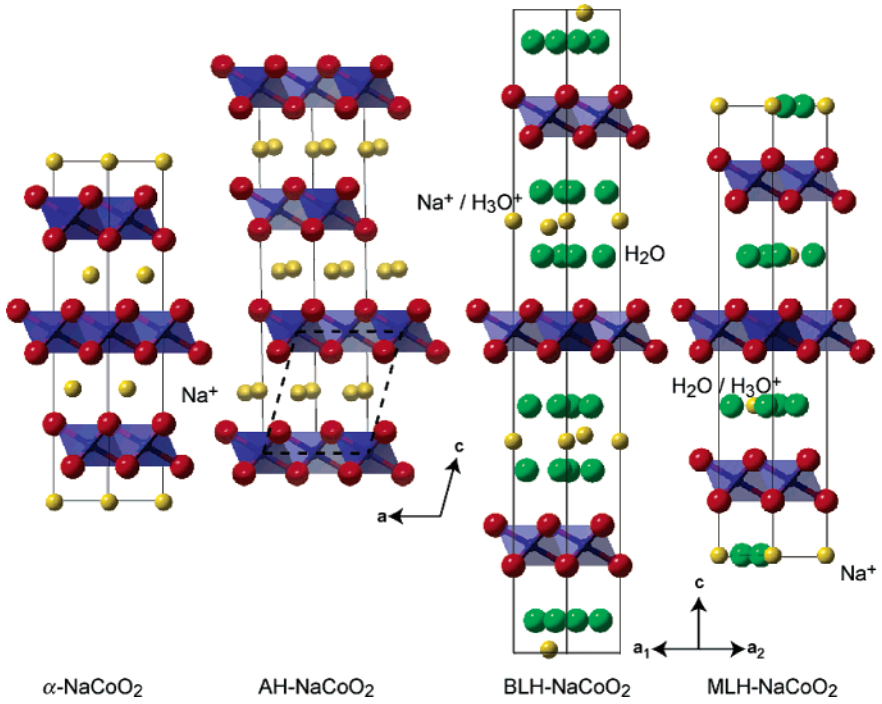

Figure 3. Crystal structures of the parent (α-), AH-, BLH-, and MLH-phases in the P3 series. Dashed lines indicate a monoclinic unit cell of the AH-Na_x-CoO_2.

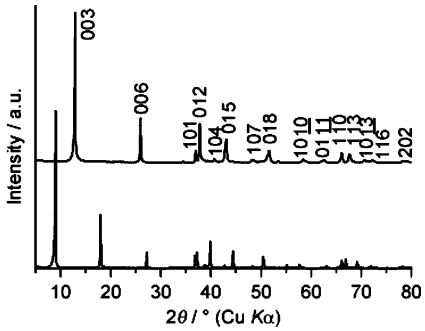

Figure 4. Powder XRD patterns for the BLH- (lower) and MLH-phases (upper).

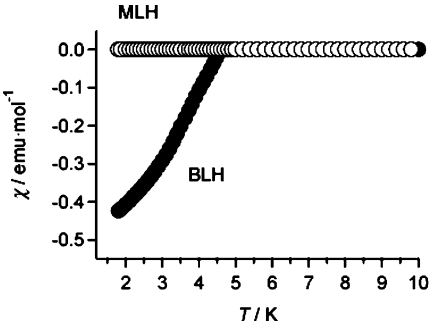

Figure 5. Magnetic susceptibility (χ) of P3 BLH- and MLH-phases as a function of absolute temperature (T).

The two structure models produce quite different structure factors, and only the P3 structure gave reasonable refinement results. This means that the formation of the MLH-phase involved the interlayer shrinkage without the lateral gliding of the CoO_2 sheets. Figure 2b shows the Rietveld refinement pattern, and Table 2 lists the structure parameters for the MLH-phase refined on the basis of the P3 structure model. The resultant R factors were satisfactorily low to support the structure model.

Electron-density distribution displayed in Figure 6 resulting from the MEM analysis revealed that electrons corresponding to the guest species are spread over the intermediate planes between the CoO_2 layers, on which maximum number density was observed at 3*a* sites. Na^+ ions occupy the 3*a* sites in the refinement, which are the midpoints between two oxygen atoms facing each other in the adjacent CoO_2 layers. The O−O distance over the gallery was 4.978(10) Å. Since ionic radius of an O^{2-} ion is 1.4 Å, the maximum radius of the species that can reside at the midpoint should be 1.1 Å. The Na^+ ions can fit to this interstice, whereas H_3O^+ ions and H_2O molecules are too large. They occupy the trigonal prismatic sites; 6*c* ($^2/_3$, $^1/_3$, 0) sites at the centers of the trigonal prisms were split into 18*h* (x, $^x/_2$, z; $x \approx 0.43$ and $z \approx 0.00$) sites in the final refinement. This arrangement of the guest species is very similar to that in the P2 MLH-phase.[5] The O−O distance over the gallery in the P2 MLH-phase was 5.078(15) Å, which is almost the same as that in the P3 MLH-phase.

Guest Species in the Hydrates. In general, the guest species such as Na^+ and H_3O^+ ions and H_2O molecules do not make a large contribution to the XRD data, because they are composed of light elements. The guest species are highly disordered in the arrangement, and moreover, all the species have the same number of electrons: 10 each. This situation limits detailed discussion on how the guest species are distributed in the interlayer gallery. On the other hand, Raman spectroscopy is sensitive not only to chemical species but also to site symmetry of the species. In fact, although the arrangements of the guest species in the P3 BLH- and P3 MLH-phases are considered to be very similar to those in the P2 counterparts, Raman spectra of the former were different from the latter. This is helpful to obtain a deeper understanding of the configuration of the interlayer guests.

Table 2. Fractional Coordinates, Occupancies, *g*, and Isotropic Atomic Displacement Parameters, *U*, for the P3 MLH-Phase[a]

atom	site	*x*	*y*	*z*	*g*	*U*/Å^2
Co	3*b*	1/3	2/3	1/6	1	0.066(8)
O	6*c*	0	0	0.1209(3)	1	0.0146(11)
Na	3*a*	0	0	0	0.359	0.070(4)
M (H_2O/H_3O)	18*h*	0.430(6)	= *x*(M)/2	0.0013(14)	0.0987	0.031(6)

[a] Space group $R\bar{3}m$ (No. 166); $a = 2.8261(3)$ Å, $c = 20.588(4)$ Å; $R_{wp} = 11.93\%$ ($S = 1.99$), $R_p = 9.16\%$, $R_B = 1.93\%$, and $R_F = 1.43\%$. M denotes a virtual chemical species having a mean scattering amplitude of H_3O^+ ions and H_2O molecules. The atomic scattering factors for a H_3O^+ ion and a H_2O molecule were set equal to the sums of one oxygen atom and the corresponding numbers of hydrogen atoms.

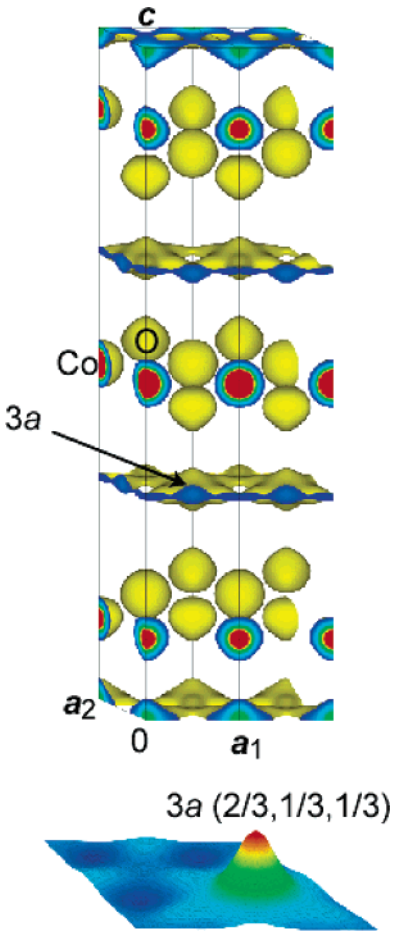

Figure 6. Three-dimensional image of electron density distribution in 2 × 1 × 1 unit cells of the P3 MLH-phase (upper) and a bird's-eye view of the number density distribution on the (0 0 3) plane (lower). Isosurfaces corresponding to number density of electrons of 1.0 Å^{-3} are displayed in the three-dimensional image.

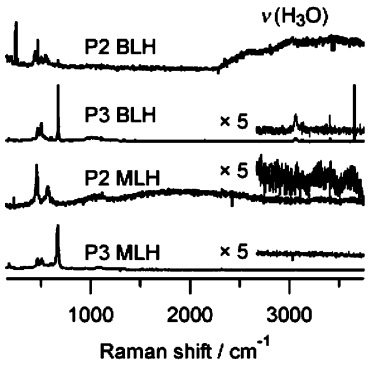

Figure 7. Raman spectra for the samples. Dotted lines are expansion of the spectra by five times.

Figure 7 shows Raman spectra for the BLH- and MLH-phases with P2 and P3 structures. The Raman spectra of the phases exhibited intense modes and broad bands in the wavenumber regions lower than 800 cm^{-1} and higher than 2000 cm^{-1}, respectively. The former are attributable to vibrations of the host lattices, while the latter are assignable to molecular vibration of −OH groups. The anhydrous phases did not give any Raman peaks in the high-frequency region indeed (not shown). This study was focused on the changes in the high-frequency region involved with the motion of −OH groups. The detailed analysis of the low-frequency spectra will be discussed elsewhere.

The broad bands observed for the P2 BLH-phase included a peak at ca. 3000 cm^{-1}. This peak has been assigned as a characteristic stretching mode in H_3O^+ ions, $\nu(H_3O)$,[22] and thus, at least part of the other poorly resolved bands should be originated from the H_2O molecules. The former was also clearly observed for the P3 phase, whereas the latter were largely suppressed.

Because the H_2O molecules reside at the 18*h* sites in the P3 BLH-phase, which are Raman-active as listed in Table 3, it is not the Raman-inactiveness but the high two-dimensionality of the BLH-phase that attenuates their Raman modes in the P3 BLH-phase. High two-dimensionality causes degeneration of out-of-plane modes, i.e., *A* and *B* modes. Therefore, six *E* modes out of nine from the H_2O molecules should be clearly observed for the P2 BLH-phase, while half of the six modes will be suppressed for the P3 BLH-phase, which may be the reason for the disappearance of the Raman modes.

Dehydration from the P3 BLH-phase quenched the $\nu(H_3O)$ Raman mode. The structure analysis above revealed that the H_3O^+ ions occupy the same 18*h* sites as the H_2O molecules in the P3 MLH-phase; Raman modes from the species sitting there (see Table 4) are suppressed by the high two-dimensionality as described above. This may be the reason for the disappearance of the Raman mode from the H_3O^+ ions. Another conceivable explanation for the disappearance of the Raman mode from the H_3O^+ ions is that the H_3O^+ ions are deformed or dissociated into protons and H_2O molecules in the MLH-phase.

When a H_2O molecule is inserted near a Brønsted acid site of an oxide framework, it will form a H_3O^+ ion, or protonated water, by attracting a proton from the acid site, or remain as a H_2O molecule hydrogen-bonded to the acid site. In fact, both of them were found in a zeolite, HSAPO-34.[23] This result suggests that a H_3O^+ ion in an oxide framework may be dissociated into a proton and a H_2O molecule, to the contrary, by interaction with an oxygen atom in the framework. Even if the H_3O^+ ion is not dissociated,

(22) Wilkins, R. W. T.; Mateen, A. *Am. Miner.* **1974**, *59*, 811.
(23) Smith, L.; Cheetham, A. K.; Morris, R. R.; Marchese, L.; Thomas, J. M.; Wright, P. A.; Chen, J. *Science* **1996**, *271*, 799.

Table 3. Raman-Active Modes in the BLH-Phases (Fractional Coordinates for P2 BLH- and P3 BLH-Phases Are Quoted from Refs 18 and 12, Respectively)

	P2 BLH		P3 BLH	
species	position	Raman modes	position	Raman modes
Co	2*a* (0, 0, 0)		3*b* ($^1/_3$, $^2/_3$, $^1/_6$)	
O	4*f* ($^1/_3$, $^2/_3$, *z*; $z \approx 0.05$)	$A_{1g} + E_{1g} + E_{2g}$	6*c* (0, 0, *z*; $z \approx 0.14$)	$A_{1g} + E_g$
Na^+/H_3O^+	4*e* (0, 0, *z*; $z \approx 0.24$)	$A_{1g} + E_{1g} + E_{2g}$	6c ($^2/_3$, $^1/_3$, *z*; $z \approx 0.00$)	$A_{1g} + E_g$
	2*d* ($^2/_3$, $^1/_3$, $^1/_4$)	E_{2g}		
H_2O	12*k* (*x*, 2*x*, *z*; $x \approx 0.14$, $z \approx 0.17$)	$A_{1g} + A_{2g} + B_{2g} + 3E_{2g} + 3E_{1g}$	18*h* (*x*, 2*x*, *z*; $x \approx 0.18$, $z \approx 0.05$)	$2A_{1g} + A_{2g} + 3E_g$
	12*k* (*x*, $^x/_2$, *z*; $x \approx 0.90$, $z \approx 0.17$)	$A_{1g} + A_{2g} + B_{2g} + 3E_{2g} + 3E_{1g}$	18*h* (*x*, $^x/_2$, *z*; $x \approx 0.42$, $z \approx 0.05$)	$2A_{1g} + A_{2g} + 3E_g$

Table 4. Raman-Active Modes in the MLH-Phases (Fractional Coordinates for P2 MLH-phases Are Quoted from Ref 11)

	P2 MLH		P3 MLH	
species	position	Raman modes	position	Raman modes
Co	2*a* (0, 0, 0)		3*b* ($^1/_3$, $^2/_3$, $^1/_6$)	
O	4*f* ($^1/_3$, $^2/_3$, *z*; $z \approx 0.07$)	$A_{1g} + E_{1g} + E_{2g}$	6*c* (0, 0, 0.12)	$A_{1g} + E_g$
Na^+	2*c* ($^1/_3$, $^2/_3$, $^1/_4$)		3*a* (0, 0, 0)	
H_2O/H_3O^+	6*h* (*x*, 2*x*, $^1/_4$; $x \approx 0.18$)	$A_{1g} + A_{2g} + E_{1g} + 2E_{2g}$	18*h* (*x*, $^x/_2$, *z*; $x \approx 0.43$, $z \approx 0.00$)	$2A_{1g} + A_{2g} + 3E_g$

it may be deformed to some extent by the interaction. Actually, the H_3O^+ ion in the zeolite was deformed; one of the O−H bonds was longer (1.14 Å) than the other two (0.95 and 0.91 Å).

Such deformation or dissociation of a H_3O^+ ion should take place when it is located near a framework oxygen atom. It is needless to say that the prominent difference between the BLH- and MLH-phases is in the interlayer distance. Although the H_3O^+ ions are considered to reside on the intermediate planes between the CoO_2 layers in both of the phases, the shrinkage of the *c*-axis upon the dehydration decreased the distance between the H_3O^+ ions and oxygen atoms in the CoO_2 layers. The O (in a CoO_2 layer)−O (in an H_3O^+ ion) distance decreased from 4.181(10) Å in the P3 BLH-phases[11] to 2.68(3) Å in the MLH-phases. The distance in the MLH-phases is coincident with those reported for the zeolite (2.50 and 2.70 Å for the dissociated H_3O^+ ion and 2.51 Å for the deformed H_3O^+ ion). Therefore, it is possible that such dissociation or deformation takes place in the MLH-phases, which results in the disappearance of the H_3O^+ Raman mode.

The H_3O^+ ions in the P2 MLH-phase are in the same situation; they are apart from the oxygen atoms in the CoO_2 layers by 2.655(10) Å.[5] The Raman spectrum for the P2 MLH-phase had several bands from H_2O molecules in the wavenumber region higher than 3200 cm^{-1}, as shown in Figure 6. Since the H_3O^+ ions are at the same crystallographic sites as the H_2O molecules, $\nu(H_3O)$ mode should be observed in the spectra as well; however, it was hardly observed. This may also suggest the deformation or dissociation of the H_3O^+ ions in the MLH-phases.

Indeed, structure of framework will greatly influence the degree of such dissociation or deformation. Only hydrogen-bonded water was found in a different kind of zeolite, H-ZSM-5.[24] Structural study of H_3O^+ ions incorporated in a NASICON framework revealed that the shape of the H_3O^+ ions changed upon the phase transition;[25] that is, change in the framework modifies the shape of the H_3O^+ ion. The negligibly small peak from H_3O^+ ion may suggest a high degree of dissociation of the H_3O^+ ions into H_2O molecules and protons in the MLH-phases; the latter may be bonded to oxygen atoms in CoO_2 layers to form bridging hydroxyl groups. Further study in combination with neutron diffraction is necessary for final conclusion on the guest structure.

The hydrogen-bonding between the hydroxyl groups and the H_2O molecules may be the reason the positions of H_2O molecules are not the center of the trigonal prisms, 2*b* (0, 0, $^1/_4$) and 2*d* ($^2/_3$, $^1/_3$, $^1/_4$) for P2 and 6*c* ($^2/_3$, $^1/_3$, 0) for P3, but shifted to their edges. In addition, the formation of the hydroxyl groups may be the answer to the question of why the superconductivity disappears by the dehydration, although interlayer distance of 6.9 Å in the MLH-phases seems large enough to make the CoO_2 layers highly two-dimensional. It may modify the electronic structure of the CoO_2 layers.

Conclusions

Phases related to a superconducting phase with P3 structure were characterized by chemical analysis, XRD, and Raman spectroscopy. They are very similar to those found for cobalt oxides with P2 structure. The redox potential of the Co^{3+}/Co^{4+} couple in the CoO_2 layer plays an important role in the formation of the phases, i.e., the transformation between them. Since it will be little affected by difference in the stacking sequence of the CoO_2 layers, they are similar between the P2 and P3 systems. The results from Raman spectroscopy suggested that the H_3O^+ ions in the superconductors are deformed or dissociated upon the transformation from the bilayer-hydrate to monolayer-hydrate phases.

Acknowledgment. We thank Mr. Satoshi Takenouchi for ICP-AES and redox titration. This study was partially supported by Grants-in-Aid for Scientific Research (B) from Japan Society for the Promotion of Science (16340111).

CM047737Y

(24) Jovic, H.; Tuel, A.; Krossner, M.; Sauer, J. *J. Phys. Chem.* **1996**, *100*, 19545.

(25) Catti, M.; Ibberson, R. M. *J. Phys. Chem. B* **2002**, *106*, 11916.